PAPER

Check for updates

Thermal runaway features of large-format power lithium-ion cells under various thermal abuse patterns and capacities†

Guanlin Peng,‡[ab] Xiaodong Ling,‡[ab] Yujie Lin,[ab] Hui Jiang,[a] Mengbai Ma,[a] Anfeng Yu*[a] and Dongxu Ouyang [ID] *[c]

Herein, a comprehensive investigation is performed to research the thermal runaway features of large-format power lithium-ion cells under various heating patterns (2 kW electric heating oven and 600 W electric heating plate) and capacities (60, 150, and 180 Ah). Although the electric heating plate induces the cell to encounter thermal runaway earlier in comparison with the electric heating oven, the combustion does not appear for the former case since the compact stacking of the electric heating plate restrains the heat release of the heater such that the surrounding temperature is too low to induce the ignition of the thermal runaway combustibles. Besides that, it is interesting to find that the color of the ejected products under the electric heating plate condition becomes shallower as the thermal runaway proceeds, which implies that the ejecta in the initial of thermal runaway is mixed with quantities of solid particles and the proportion would gradually decrease. With the increase of the cell capacity, thermal runaway emerges later as a result of the greater cell height which delays the cell temperature rise, when exposed to an electric heating oven. In addition, the cell with a larger capacity demonstrates a lower peak temperature, a lower maximum temperature rise rate, a shorter combustion, a lower flame temperature, and a weaker radiation heat strength during thermal runaway; that is, less heat is released due to its violent thermal runaway behaviour. Finally, the severe explosion risk for the larger-capacity cell should be especially noted considering the larger amount of explosive gases released.

1. Introduction

As one of the most prevalent energy storage devices, lithium-ion cells are being extensively applied in electric vehicles as the power source.[1,2] Meanwhile, power lithium-ion cells are becoming more and more larger and are arranged more and more compactly to store greater energy and further extending the endurance mileage of vehicles. As a result of the huge energy density and the inherent safety defects of lithium-ion cells, the fire and/or explosion accidents of electric vehicles are frequently reported causing massive loss and bad social influence, and most roots are attributed to the thermal runaway of power lithium-ion cells.[3–5] Thereby, the thermal runaway features of

[a]SINOPEC Research Institute of Safety Engineering Co., Ltd., Qingdao, 266104, China. E-mail: yuaf.qday@sinopec.com

[b]SINOPEC National Petrochemical Project Risk As-sessment Technical Center Co., Ltd., Qingdao, 266104, China

[c]College of Safety Science and Engineering, Nanjing Tech University, Nanjing, 211816, China. E-mail: ouyang11@mail.ustc.edu.cn

† Electronic supplementary information (ESI) available. See DOI: https://doi.org/10.1039/d3ra06425e

‡ Co-first authors.

large-format power lithium-ion cells should be paid enough focus considering the great safety risk and hazard.

In comparison with traditional lithium-ion cells such as 18 650-, 21 700-format cells, the thermal runaway behaviour of large-format power lithium-ion cells would be much more dramatic and destructive.[6–11] Although the detailed size of the jet fire by a large-format power cell has not been measured yet, it can be estimated that a length of more than 3 meters can be easily attained based on the experimental phenomena.[6] According to the research of Peng *et al.*,[7] the total heat release of a fully-charged 68 Ah cell during thermal runaway could reach 6.7 MJ, while that of an 18 650-format cells with a capacity of 1.3 Ah was only 97.7 kJ.[12] Considering the thermal runaway of a large-format cell would release quantities of toxic gases, Liu *et al.*,[8] measured the gas releasing behaviour of an 243 Ah cell in the process of thermal runaway, and found that the maximum concentration for hydrogen fluoride during testing was as high as 162 mg m^{-3}, which was much greater than the Immediately Dangerous to Life or Health (IDLH) limit of hydrogen fluoride (24.6 mg m^{-3}).[13] Obviously, the thermal runaway of a large-format lithium-ion cell is accompanied with tremendous hazards as a result of the violent jet fire, great heat release and abundant toxic gases.

The triggering pattern of lithium-ion cell thermal runaway is generally summarized as three types: thermal abuse, electrical

abuse and mechanical abuse;[14,15] whereby, the thermal abuse is especially usual. The thermal abuse pattern usually dominates the cell's thermal runaway progress as a result of the heat transfer and heat dissipation difference. In addition, the capacity of lithium-ion cells is diverse that ranges from dozens of mAh to hundreds of Ah due to the varied market demand. The cell capacity that determines the energy carried by a cell impacts significantly on the thermal runaway behaviour of cells as well. To complete a comprehensive research on the thermal runaway features of large-format power lithium-ion cells under various heating patterns and capacities, the current work prepared two types of thermal abuse patterns (electric heating plate and electric heating oven) and three types of power cells with various capacities (60, 150, and 180 Ah). Crucial parameters like cell surface temperature, cell mass, thermal runaway phenomenon, radiation heat flux, flame temperature, flame morphology, gas generation, *etc.*, were collected and analyzed to deepen human's understanding on large-format power cells' thermal runaway.

2. Experimental

2.1 Cell samples

There are four kinds of large-format power cells used in this work, with capacities of 40, 60, 150, and 180 Ah. The details of these cells are listed in Table 1. Before testing, the cells were cycled twice between 2.75 and 4.2 V at a rate of 0.5C to activate them. After that, the cells were charged to 100% state of charge (SOC) and left undisturbed for 24 hours to ensure their stability during the tests.

2.2 Apparatuses and experimental design

Fig. 1(a) and (b) depict the schematic of the experimental setups with two various thermal abuse patterns, respectively. For the case with an electric heating oven, the cell and the heat insulation boards were stacked inside the fixture. An electric heating oven with a power of 2 kW was positioned below the cell with a distance of 5 cm to induce cell thermal runaway. Power cells were placed on a supporting mesh made of iron wire in tests. In terms of the case with an electric heating plate, the cell and the electric heating plate were stacked with a fixture made of stainless steel. There was a heat insulation board between the cell/plate and the fixture to avoid heat dissipation during tests. The electric heating plate had a power of 600 W. Two K-type thermocouples with a diameter of 1 mm were attached to both sides of each cell to measure its surface temperatures and the temperatures were recorded using data acquisition

equipment (NI cDAQ-9174) by a computer. An electric balance (Mettler Toledo XP10002S) was positioned below the testing platform to track the variation of cell mass. Four radiation heat flux meters (Shanghai Anyi) were arranged around the cell with distances of 30, 60, 90, and 120 cm, respectively to analyze the distribution of radiation heat flux during thermal runaway. The gas generation (hydrogen, carbon dioxide, carbon monoxide, and hydrocarbon) in the process of testing was measured *via* a gas analyzer (GT-2000). Experimental phenomena were recorded by a camera (SONY XPS160) with a resolution ratio of 25 fps and a high-speed infrared camera (Telop FAST M200) with a resolution ratio of 640 × 512 fps.

Two groups of experiments were conducted separately to research the thermal runaway features of large-format power lithium-ion cells under various heating patterns and capacities, as displayed in Table 2. Except for the researching aim, the other variables in tests were strictly controlled.

3. Results and discussion

3.1 Thermal runaway features of large-format power lithium-ion cells under various thermal abuse patterns

Fig. 2(a) and (b) illustrate the surface temperature and mass profiles for 40 Ah cells under the effect of an electric heating oven and an electric heating plate, respectively. To facilitate analysis, the initial cell mass was adjusted as 0 g. Since the oven is positioned below the cell, the surface temperatures for the both sides of the cell behave consistently until the occurrence of thermal runaway. When the cell temperature increases to approximately 168 °C, the cell safety valve opens to reduce the interior pressure of the cell. As a result of the heat taken away by the high-temperature gases, the cell temperature declines somewhat.[16–18] Meanwhile, the cell mass reduces in an accelerated manner. After that, the cell temperature continues to grow stably and then thermal runaway undergoes. A peak surface temperature higher than 750 °C and a mass loss of around 74.3 g are attained finally. In terms of the case with an electric heating plate, the temperature for the left side of the cell increases more dramatically due to the closer to the plate, in comparison with that of the right side. Different from the thermal runaway features under the oven condition, the safety valve opening almost synchronously appears with the thermal runaway. A combustion does not encounter during the whole thermal runaway process. More details can be found in the experimental phenomena displayed in Fig. 3. Due to the worse ejection behaviour, the cell experiences a more severe mass loss (314.8 g) than that under the effect of an oven. While

Table 1 The detailed information of cells

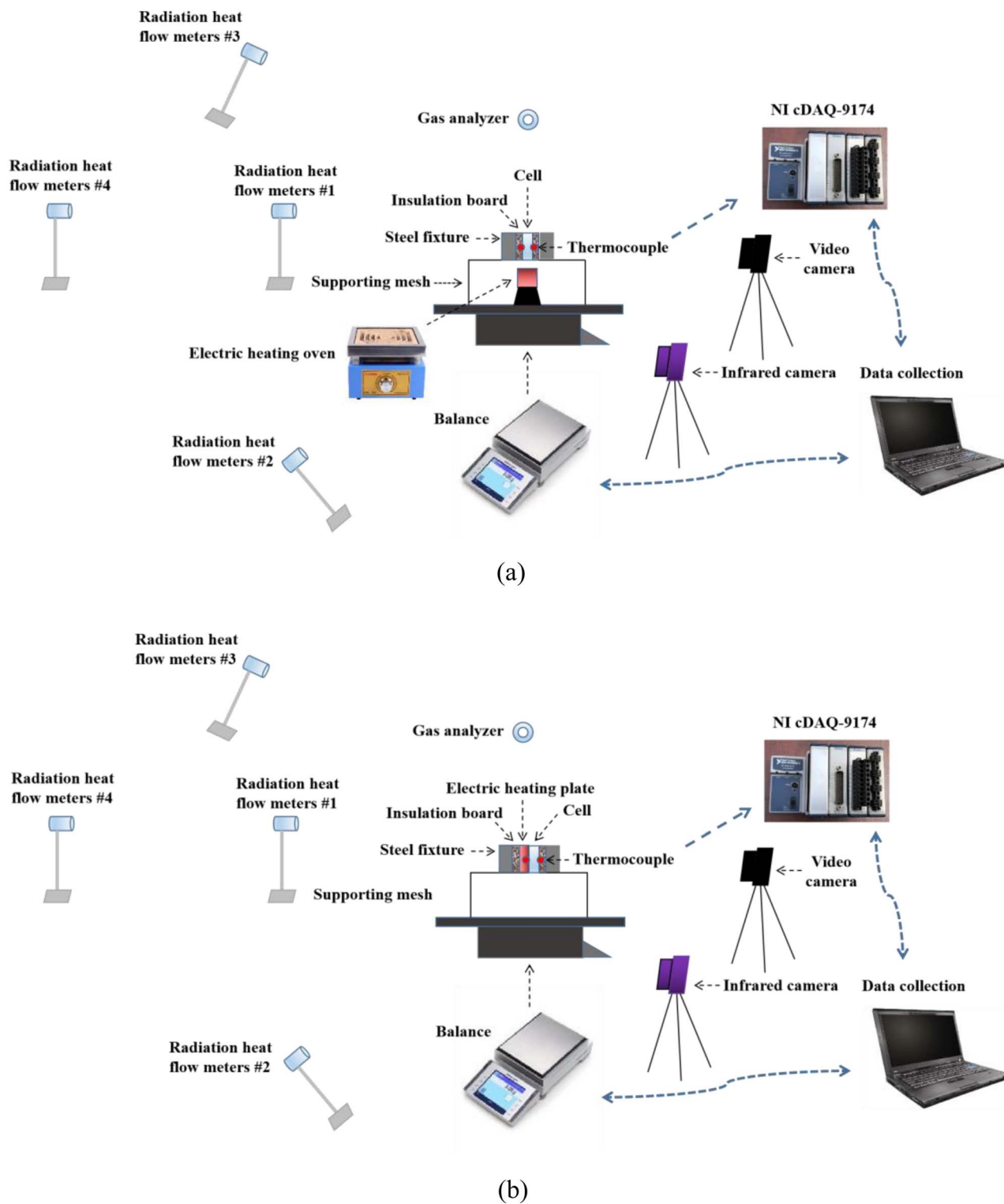| No.	Nominal capacity (Ah)	Cell size, *i.e.*, length × width × height (mm)	Cathode materials	Anode materials	Cut-off voltage (V)
1	40	145 × 25 × 90	$LiNi_{0.6}Mn_{0.2}Co_{0.2}O_2$	Graphite	4.2/2.75
2	60	170 × 30 × 70	$LiNi_{0.5}Mn_{0.3}Co_{0.2}O_2$		
3	150	220 × 45 × 80			
4	180	160 × 80 × 100			

Fig. 1 Schematic of the experimental setup: (a) electric heating oven; (b) electric heating plate.

a comparatively lower peak temperature is obtained (610 °C) because of the absent combustion.

The 40 Ah cells under the two thermal abuse patterns illustrate quite different thermal runaway behaviours. Once the safety valve opens, gray gases resulting from thermal runaway side-reactions start releasing as shown in Fig. 3(a1). Related discussion on the released gases refers to Fig. 12. When the thermal runaway emerges, a much more severe gas releasing encounters accompanied with quantities of black solid particles (the electrode material's debris under the effect of the violent

Table 2 The experimental configurations

Group no.	Test no.	Cell capacity (Ah)	SOC (%)	Thermal abuse pattern
1	1	40	100	Electric heating oven
	2			Electric heating plate
2	3	60		Electric heating oven
	4		150	
	5		180	

shock). The combustibles closer to the oven are easier ignited due to the higher temperature and then forms a stable combustion as shown in Fig. 3(a4). Eventually, the flame extinguishes with the consumption of combustibles. As for the cell with the effect of an electric heating plate, it encounters safety valve opening at the eve of thermal runaway, see Fig. 3(b1). This might be ascribed from its fiercer thermal runaway evolution, the faster side reactions and the worse gas generation result in the nearly synchronous safety valve opening and thermal runaway. There is an interesting phenomenon worthy to be emphasized that the color of the released products becomes shallow gradually as the thermal runaway progresses. It can be speculated that there are quantities of solid particles ejected in the initial period of thermal runaway, then the released product is mainly composed of thermal runaway gases and smokes as thermal runaway progresses. Even though abundant flammable products are released, a combustion does not occur as that at the oven case, which should be attributed to the relatively lower ambient temperature above the cell. This

can be confirmed by Fig. 4, where the ambient temperatures above the cell impacted by an oven are all much higher than those of the plate case.

Fig. 4 depicts the temperature profiles of the locations (0, 10, 20, and 40 cm above the cell) in the process of thermal runaway for 40 Ah cells under the effect of the two thermal abuse patterns. The temperatures of the fixed locations above the cell impacted by an electric heating oven increase synchronously with the cell temperature. After 400 s, the temperatures above the cell rise in an accelerated manner owing to the worsened side reactions inside the cell. The gas flow after the safety valve opening would take away lots of heat so that the temperatures above the cell decline somewhat. When the thermal runaway occurs, the temperatures of all four locations dramatically increase, with the growing extent reduces as the height rises. Whereby, the location 0 cm above the cell demonstrates a maximum temperature of 708 °C. Since both the electric heating plate and the cell are tightly stacked inside the fixture, the according heat dissipation is suppressed so that the temperatures above the cell are comparatively stable until the emergence of thermal runaway. Consistent with the analysis of the experimental phenomena, the temperature profiles of the fixed locations in the process of thermal runaway can be divided into two phases, corresponding to the early stage that quantities of solid particles are mixed and the later stage which releases abundant gray gases and smokes. It is apparent that the released products in the later thermal runaway possess a significantly higher temperature. Due to the absence of combustion, the temperatures of the locations 10, 20, and
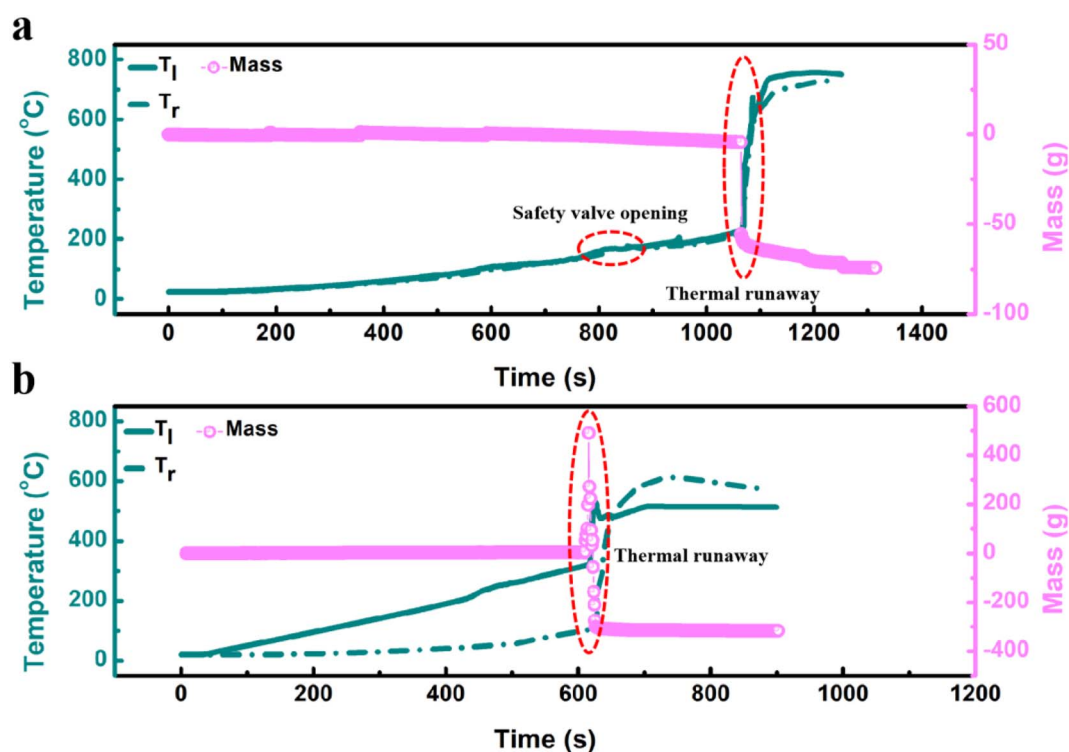

Fig. 2 The surface temperature and mass profiles for 40 Ah cells under the effect of (a) electric heating oven and (b) electric heating plate.
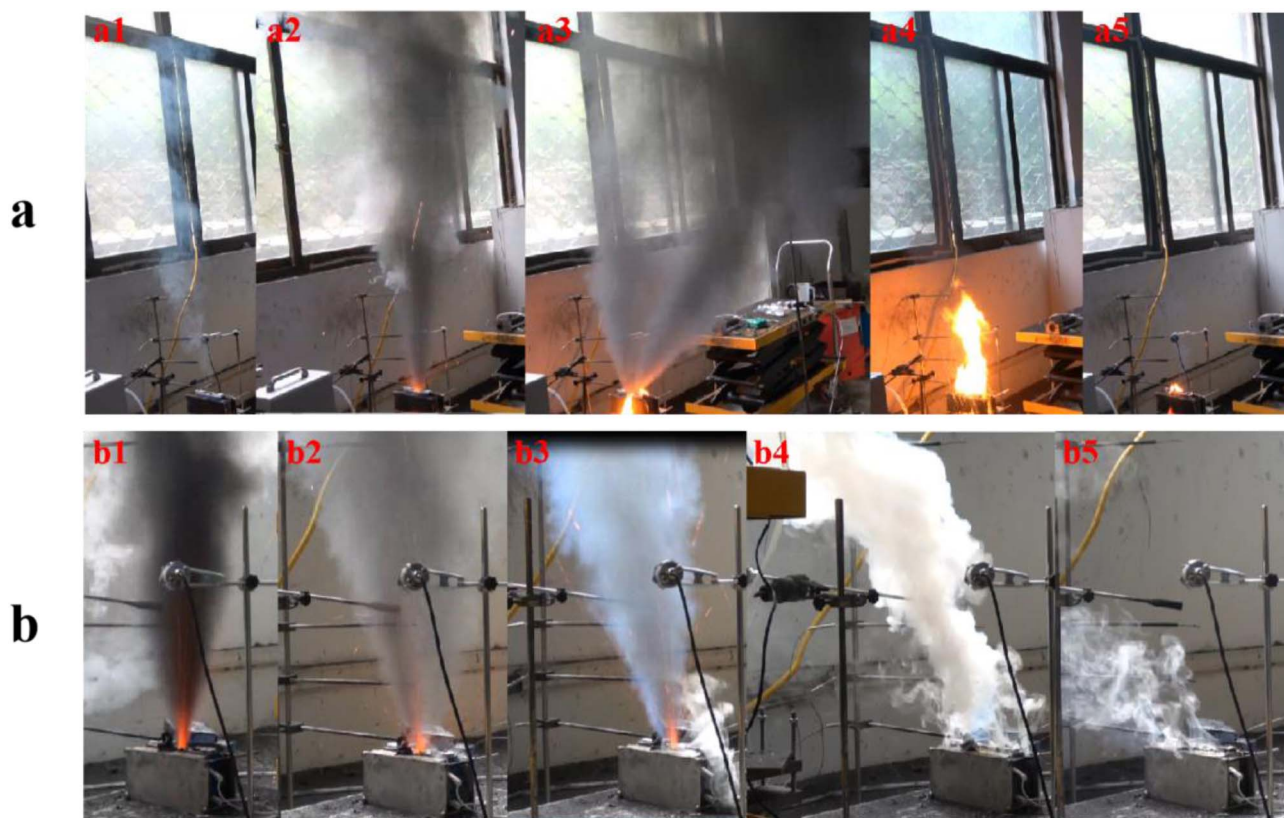
Fig. 3 The typical thermal runaway behaviour for 40 Ah cells under the effect of (a) electric heating oven and (b) electric heating plate.
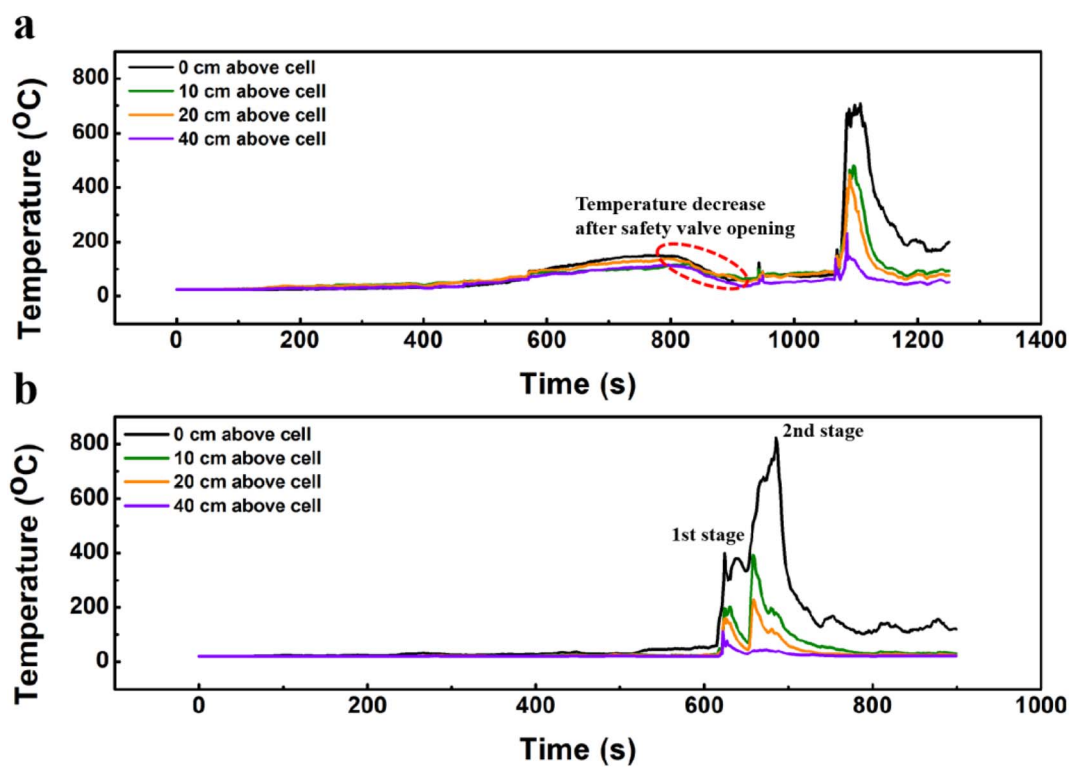

Fig. 4 The temperature profiles of the fixed locations in the process of thermal runaway for 40 Ah cells under the effect of (a) electric heating oven and (b) electric heating plate.

40 cm above the cell under the plate case are all evidently lower than those under the oven condition.

Considering the existence of the flame for the condition under the effect of an oven, the radiation heat flux, flame morphology, and flame temperature will be further analyzed in follows to provide a comprehensive understanding on the thermal runaway features of power cell thermal runaway. Fig. 5(a) compares the radiation heat flux profiles of the locations 30, 60, 90, and 120 cm away from the cell in the process of thermal runaway. In comparison with the positions 30, and 60 cm away from the cell, the radiation heat flux strength of the positions 90, and 120 cm away from the cell is much more weak. The peak radiation heat flux of the four locations is 4.08, 9.00, 0.88, and 0.45 kW m^{-2}, respectively. After integrating the radiation heat flux curves, the total radiation heat strength can be obtained. Fig. 5(b) displays the corresponding fitting results between the total radiation heat strength and the squared distance. As can be seen, there is an exponential decrease in the total radiation heat strength as the squared distance increases. This is in accordance with the fact that the radiation heat flux of

traditional combustion is inversely proportional to the radiation distance.[19–21]

The variations of the flame morphology in the process of thermal runaway are depicted in Fig. 5(c). Obviously, the flame height is comparatively greater than its width. Due to the ejection inertia of the combustibles, the maximum length of the flame appears approximately 10 s after the flame generates, which is longer than 50 cm. Thereafter, the flame size shrinks gradually as the combustion proceeds. Besides that, the evolution of the mean flame temperature in the process of thermal runaway is obtained *via* an infrared camera and is further presented in Fig. 5(d). As shown, the maximum value of the mean flame temperature also appears at around 10 s later the formation of the flame, which is as high as 2307 °C. Thereafter, the mean flame temperature declines and fluctuates around 1200 °C. As the shrink of the flame, the mean flame temperature reduces as well. The whole combustion lasts approximately 80 s. In summary, both the strength and amplitude of the thermal runaway combustion for the 40 Ah cell under the effect of the thermal abuse herein would reach the peak after an evolution of about 10 s.
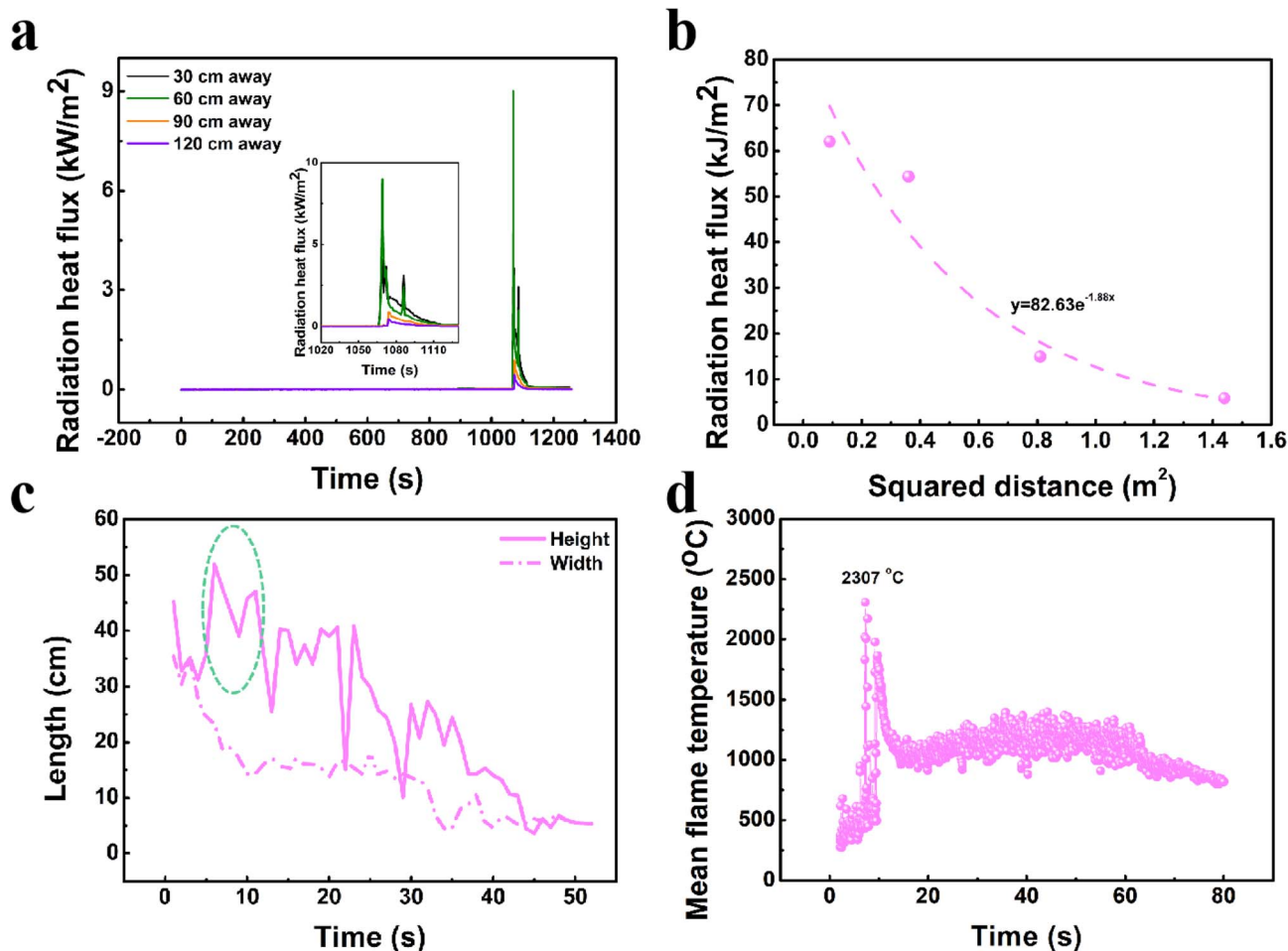

Fig. 5 Thermal runaway features for 40 Ah cells under the effect of an electric heating oven: (a) the radiation heat flux profiles of the fixed locations in the process of thermal runaway; (b) the fitting relationship between the radiation heat flux and squared distance; (c) the variations of the flame height and width in the process of thermal runaway; (d) the variations of the mean flame temperature in the process of thermal runaway.

3.2 Thermal runaway features of large-format power lithium-ion cells under various capacities

Given that the thermal runaway features of large-format power cells are demonstrated more comprehensively under the effect of an electric heating oven, the thermal runaway of power cells with various capacities would be induced *via* the electric heating oven. Fig. 6 compares the surface temperature profiles of 60, 150, and 180 Ah cells in the process of thermal runaway. Due to the lower height for the 60 and 150 Ah cells (see Table 1), both the thermocouple and the cell center are closer to the oven, such that these two cells demonstrate faster temperature rise than the 180 Ah cell. This phenomenon is in accordance with the authors' previous finding,[22] where the thermal runaway proceeding of 18 650-, 22 650-, and 26 650-format cells slowed in order when exposed to the same thermal abuse. In the end, thermal runaway occurs at 967, 1176, and 2163 s corresponding to the 60, 150, and 180 Ah cells, respectively. Table 3 summarizes several crucial parameters of thermal runaway for the three types of cells. As the cell capacity increases, it can be found that the critical temperature to thermal runaway declines gradually, while both the maximum temperature and the maximum temperature rise rate grow. These crucial parameters imply that the 60Ah cell possesses more severe thermal runaway hazards than the other two cells. This might ascribe to two reasons: first, the 60 Ah cell's center is closer to the oven below so that its thermal runaway evolves in an accelerated manner; second, with the increase of the cell capacity, the thermal runaway behaviour would be more dramatic which inhibiting
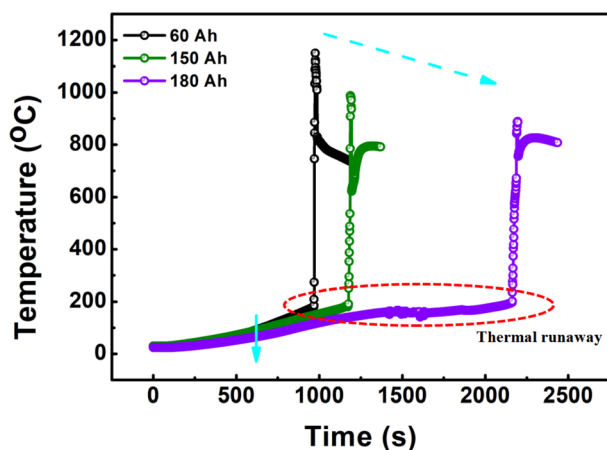

Fig. 6 The surface temperature profiles in the process of thermal runaway for 60, 150, and 180 Ah cells under the effect of an electric heating oven.
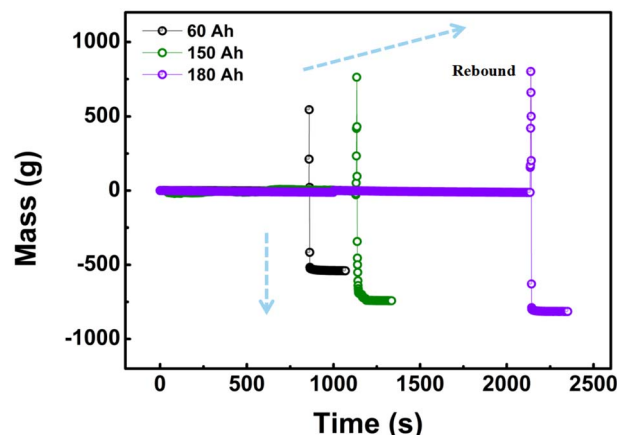

Fig. 7 The mass profiles in the process of thermal runaway for 60, 150, and 180 Ah cells under the effect of an electric heating oven.

the thermal runaway reactions so that less heat is generated, that can be verified by the lasting time of flame as depicted in the ESI (Fig. S1).† The finding here might be against with the common perception that a power cell with a larger capacity would be more dangerous and it suggests that cell thermal runaway is a complicated process correlating with cell component, format, SOC, inducing pattern, *etc.*, a larger capacity does not always bring about an earlier thermal runaway.

Fig. 7 displays the mass profiles of the three types of cells in the process of thermal runaway. As the cell capacity rises, it is shown that the cell experiences a more severe rebound when thermal runaway encounters and a worse mass loss during tests. This indicates that although the larger-capacity cell appears thermal runaway later, its thermal runaway behaviour is more violent and destructive. The dramatic thermal runaway severity suppresses the evolution of thermal runaway reactions as well.

The temperature profiles of the locations 0, 10, 20, and 40 cm above the cell in the process of thermal runaway are depicted in Fig. 8. The ambient temperatures above the cell increase slowly before thermal runaway, then they all grow dramatically under the effect of the thermal runaway flame, which could reach above 1000 °C. In the initial, the temperatures of the four locations behave similarly since the flame could fully cover the four thermocouples. With the degradation of the flame, the location's temperature declines as the height grows. In addition, it can be observed that the combustion lasting time during thermal runaway reduces gradually with the increasing the cell capacity; moreover, the temperature at the same location seems to be somewhat lower for the case with a larger capacity

Table 3 A list of thermal runaway parameters

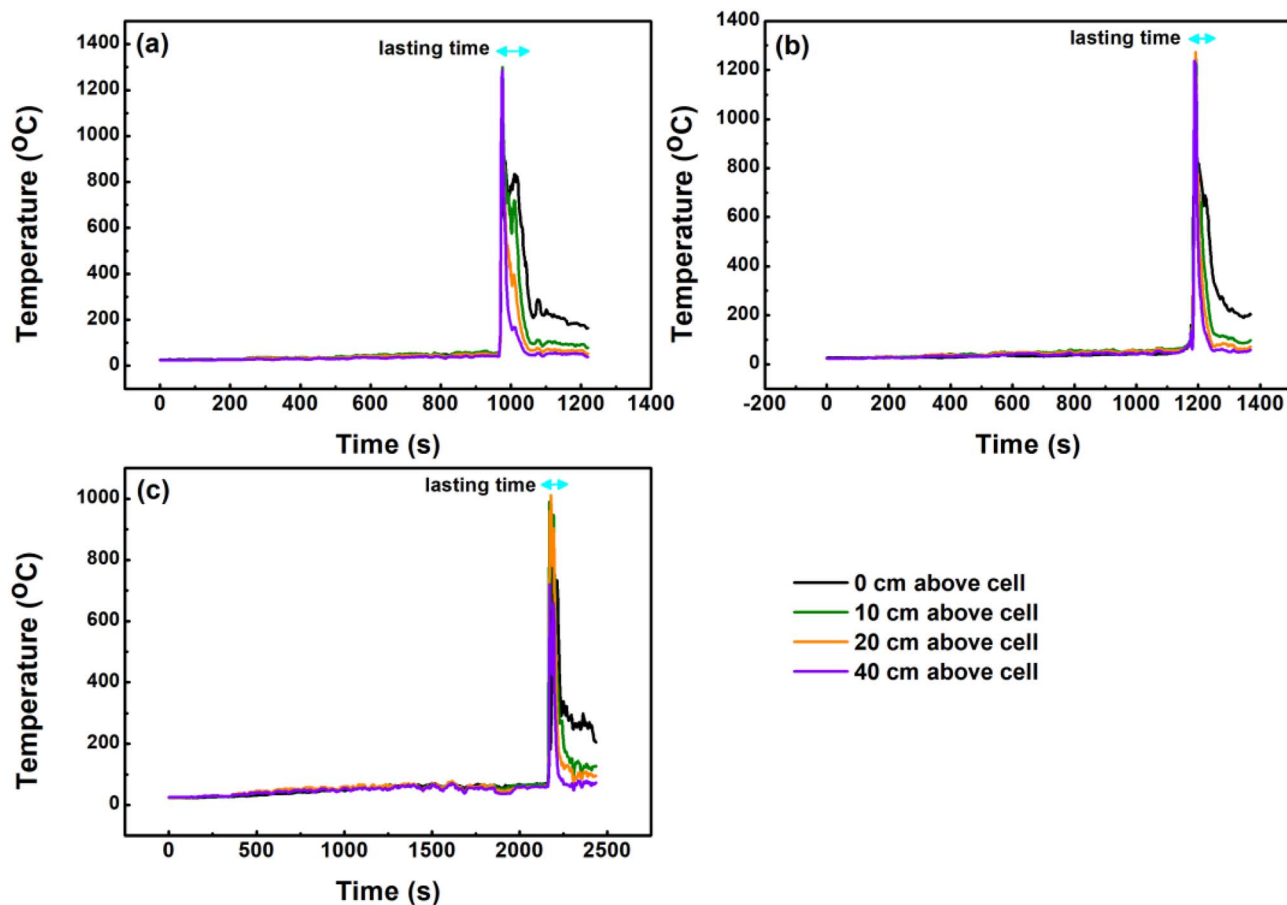| Cell	Time to thermal runaway (s)	Temperature to thermal runaway (°C)	Maximum temperature (°C)	Maximum temperature rise rate (°C min^{-1})
60 Ah	967	189.4	1149.5	28 325
150 Ah	1176	191.5	988.0	14 914
180 Ah	2163	202.2	889.1	10 269

Fig. 8 The temperature profiles of the fixed locations in the process of thermal runaway for (a) 60, (b) 150, and (c) 180 Ah cells under the effect of an electric heating oven.

especially for the 180 Ah cell. It can be speculated the severity of thermal runaway for the larger-capacity cell limits the combustion, the phenomenon of incomplete combustion might be worse.

Fig. 9 shows the radiation heat flux profiles of the locations 30, 60, 90, and 120 cm away from the cell in the process of thermal runaway. Similar to the result of 40 Ah cells, the strength of the radiation heat flux for the 30 and 60 cm locations is much greater than that of the 90 and 120 cm locations. Considering the coverage of the flame, the difference between 30 and 60 cm locations is relatively minor. Besides that, it can be found that the radiation heat strength declines gradually with the increase of the cell capacity, with peak radiation heat flux of 74.6, 70.2, and 49.0 kW m^{-2} corresponding to the 60, 150, and 180 Ah cells, respectively. This is consistent to the results of the cell surface temperature and flame temperature above; *i.e.*, the heat release and combustion strength during thermal runaway for the larger-capacity cell is comparatively weaker. After integrating the radiation heat flux curves, the total radiation heat flux of the fixed locations for the three kinds of cells is demonstrated in Fig. 10. Except for the 30 cm position, the total radiation heat flux of the other three positions still illustrates an exponential decrease with the squared distance. Moreover, with

the declining the cell capacity, a more dramatic degradation is displayed as the distance grows due to the much more intense radiation heat flux at the location closer to the cell.

The variation of the flame morphology in the process of thermal runaway is unveiled in Fig. 11. Similarly, the maximum flame height for all three kinds of cells still appears at the initial of combustion, which is greater than 120 cm (much more noticeable than that of the 40 Ah cell, ~50 cm). That is, the thermal runaway intensity of 60, 150, and 180 Ah cells is much worse than the 40 Ah cell. After that, both the flame height and width shrink gradually as the combustion goes. Whereby, the flame height of the 180 Ah cell degrades especially faster, followed by the 150 and 60 Ah cells.

Finally, the gas release behaviour involving hydrogen, carbon dioxide, carbon monoxide, and hydrocarbon for the three types of cells during thermal runaway is detected by a gas analyzer and is displayed in Fig. 12. In consistent with the mass loss result, a worse gas release is revealed in the case with a larger capacity. Among the four kinds of gases, hydrogen accounts for the largest proportion of all three cells, followed by carbon dioxide, hydrocarbon, and carbon monoxide. Even though the combustion and heat release for the larger-capacity cell is comparatively weaker, its explosion risk during thermal
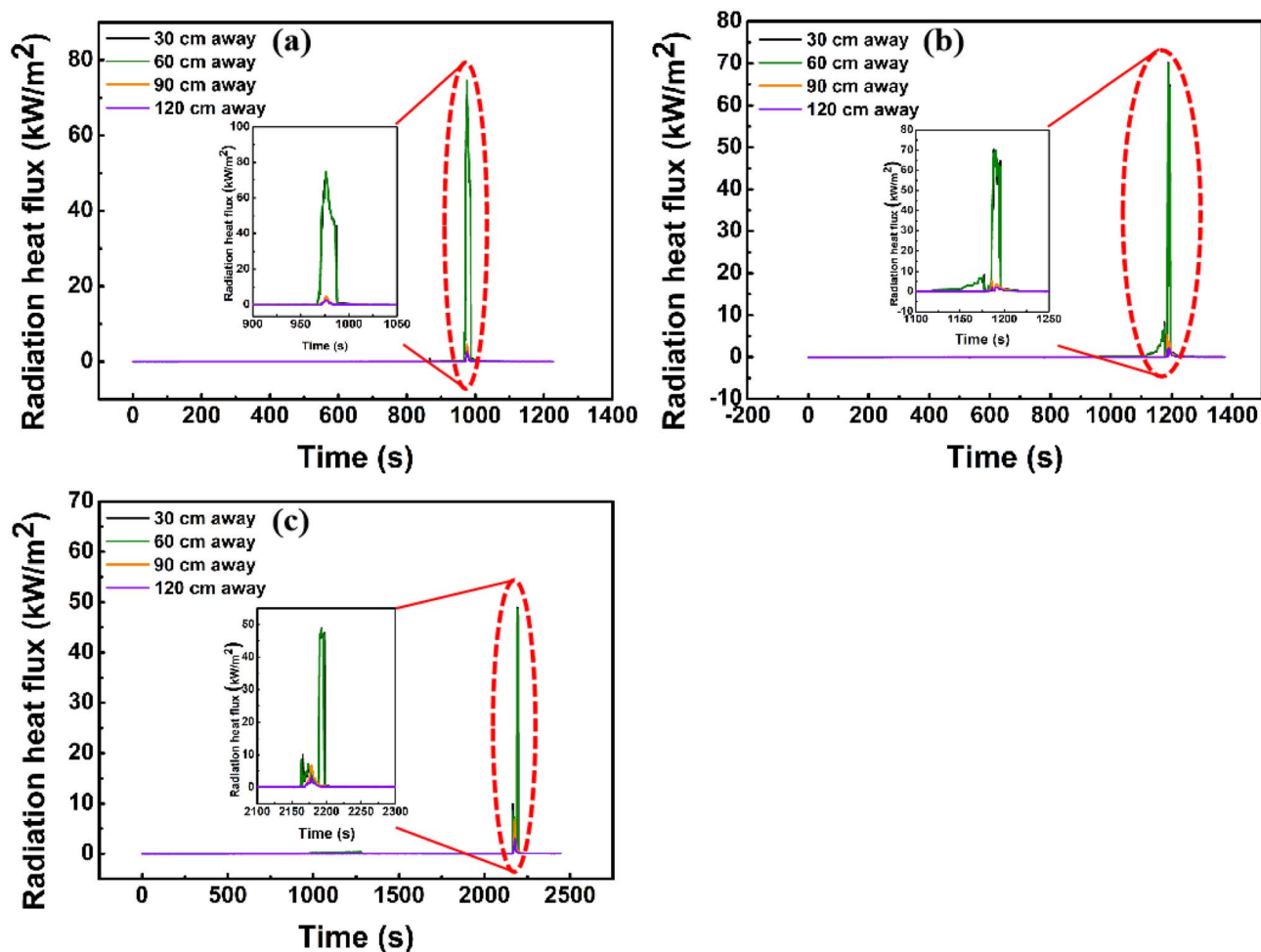
Fig. 9 The radiation heat flux profiles of the fixed locations in the process of thermal runaway for (a) 60, (b) 150, and (c) 180 Ah cells under the effect of an electric heating oven.
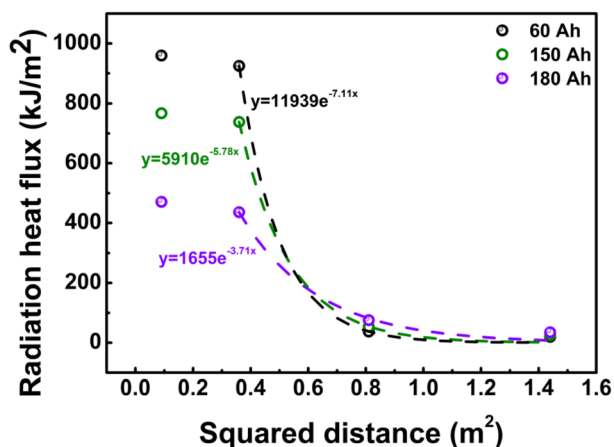

Fig. 10 The fitting relationship between the radiation heat flux and squared distance for 60, 150, and 180 Ah cells under the effect of an electric heating oven.
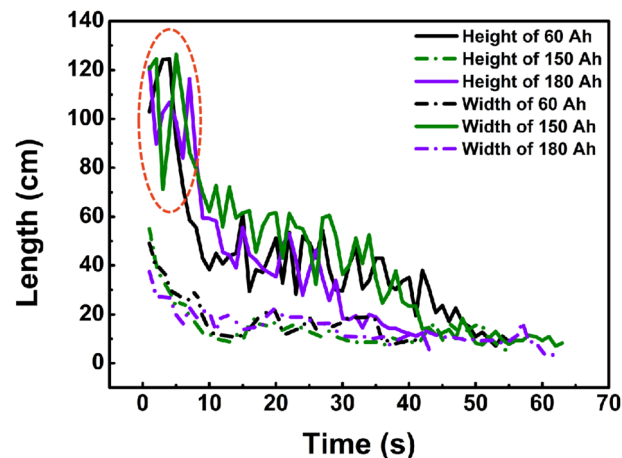

Fig. 11 The variations of the flame height and width in the process of thermal runaway for 60, 150, and 180 Ah cells under the effect of an electric heating oven.

runaway cannot be neglected considering the severer generation of explosive gases such as hydrogen, carbon monoxide, hydrocarbon, *etc.* In addition, the released gas during thermal runaway generally contains electrolyte evaporation under the effect of high temperatures. Due to the limit of instruments, the according content will not be discussed here.
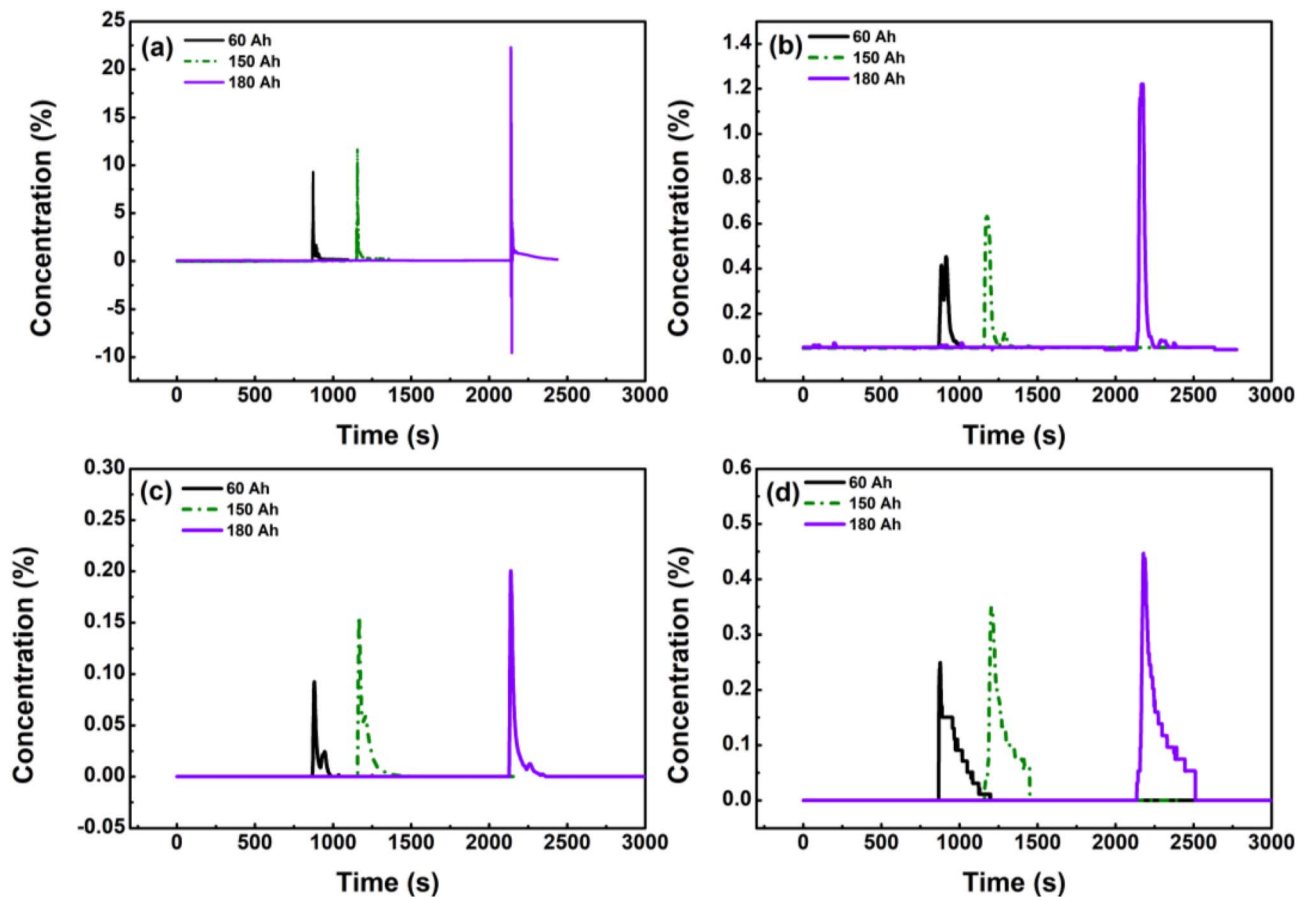
Fig. 12 The (a) hydrogen, (b) carbon dioxide, (c) carbon monoxide, and (d) hydrocarbon concentration profiles of the fixed cells in the process of thermal runaway under the effect of an electric heating oven.

4. Conclusions

Given the university of large-format power lithium-ion cells, the thermal runaway features of them under abusive conditions are worthy of more attention. The present study explored the thermal runaway behaviour of large-format power cells under various thermal abuse patterns and capacities by analyzing key parameters such as cell surface temperature, cell mass, thermal runaway phenomenon, radiation heat flux, flame temperature, flame morphology, and gas generation. Some interesting and valuable findings are addressed below.

By comparison to the electric heating oven, the electric heating plate could induce an earlier thermal runaway due to the tight combination with the cell. Nevertheless, the compact stacking also restrains the heat release of the heater such that the temperature of the surroundings is too low to cause the ignition of the combustibles released by thermal runaway. Therefore, the combustion in the oven case is replaced by the continuous jet for the plate case, where the color of the jetted products becomes shallower gradually revealing the decline of solid particles. Under the effect of an electric heating oven, thermal runaway undergoes later with the increase of the cell capacity, as a result of the greater cell height. Due to the severity of the thermal runaway behaviour, the cell with a larger capacity

illustrates a lower peak temperature, a lower maximum temperature rise rate, a shorter combustion, a lower flame temperature, and a weaker radiation heat strength, all implying restrained heat release. In addition, the total radiation heat flux in the process of thermal runaway displays an exponential decrease with the squared distance. At last, the severe explosion risk for the larger-capacity cell should be paid enough attention, which releases more explosive gases during thermal runaway.

To conclude, this work unveiled the impact of thermal abuse patterns and cell capacities on the thermal runaway features of large-format power cells. Some data, analysis, and results presented here might guide the design, management, and emergency disposal of power cells.

Conflicts of interest

There are no conflicts to declare.

Acknowledgements

References

1 Y. Hua, S. Zhou, Y. Huang, *et al.*, Sustainable value chain of retired lithium-ion batteries for electric vehicles, *J. Power Sources*, 2020, **478**, 228753.

2 J. Wen, D. Zhao and C. Zhang, An overview of electricity powered vehicles: Lithium-ion battery energy storage density and energy conversion efficiency, *Renewable Energy*, 2020, **162**, 1629–1648.

3 J. Hong, Z. Wang, C. Qu, *et al.*, Investigation on overcharge-caused thermal runaway of lithium-ion batteries in real-world electric vehicles, *Appl. Energy*, 2022, **321**, 119229.

4 W. Gao, X. Li, M. Ma, *et al.*, Case study of an electric vehicle battery thermal runaway and online internal short-circuit detection, *IEEE Trans. Power Electron.*, 2020, **36**(3), 2452–2455.

5 L. Jiang, Z. Deng, X. Tang, *et al.*, Data-driven fault diagnosis and thermal runaway warning for battery packs using real-world vehicle data, *Energy*, 2021, **234**, 121266.

6 K. Zou, X. Chen, Z. Ding, *et al.*, Jet behavior of prismatic lithium-ion batteries during thermal runaway, *Appl. Therm. Eng.*, 2020, **179**, 115745.

7 Y. Peng, L. Yang, X. Ju, *et al.*, A comprehensive investigation on the thermal and toxic hazards of large format lithium-ion batteries with LiFePO$_4$ cathode, *J. Hazard. Mater.*, 2020, **381**, 120916.

8 P. Liu, Y. Li, B. Mao, *et al.*, Experimental study on thermal runaway and fire behaviors of large format lithium iron phosphate battery, *Appl. Therm. Eng.*, 2021, **192**, 116949.

9 C. Xu, F. Zhang, X. Feng, *et al.*, Experimental study on thermal runaway propagation of lithium-ion battery modules with different parallel-series hybrid connections, *J. Cleaner Prod.*, 2021, **284**, 124749.

10 O. Willstrand, M. Pushp, P. Andersson, *et al.*, Impact of different Li-ion cell test conditions on thermal runaway characteristics and gas release measurements, *J. Energy Storage*, 2023, **68**, 107785.

11 Z. Jia, L. Song, W. Mei, *et al.*, The preload force effect on the thermal runaway and venting behaviors of large-format prismatic LiFePO$_4$ batteries, *Appl. Energy*, 2022, **327**, 120100.

12 D. Ouyang, Y. He, M. Chen, *et al.*, Experimental study on the thermal behaviors of lithium-ion batteries under discharge and overcharge conditions, *J. Therm. Anal. Calorim.*, 2018, **132**, 65–75.

13 R. Krebs, J. Owens and H. Luckarift, Formation and detection of hydrogen fluoride gas during fire fighting scenarios, *Fire Saf. J.*, 2022, **127**, 103489.

14 D. Ouyang, M. Chen, J. Weng, *et al.*, Exploring the thermal stability of lithium-ion cells via accelerating rate calorimetry: A review, *J. Energy Chem.*, 2023, **81**, 543–573.

15 X. Feng, M. Ouyang, X. Liu, *et al.*, Thermal runaway mechanism of lithium ion battery for electric vehicles: A review, *Energy Storage Mater.*, 2018, **10**, 246–267.

16 C. Zhao, T. Wang, Z. Huang, *et al.*, Experimental study on thermal runaway of fully charged and overcharged lithium-ion batteries under adiabatic and side-heating test, *J. Energy Storage*, 2021, **38**, 102519.

17 Y. Liu, P. Sun, S. Lin, *et al.*, Self-heating ignition of open-circuit cylindrical Li-ion battery pile: Towards fire-safe storage and transport, *J. Energy Storage*, 2020, **32**, 101842.

18 D. Ouyang, J. Weng, M. Chen, *et al.*, What a role does the safety vent play in the safety of 18650-size lithium-ion batteries?, *Process Saf. Environ. Prot.*, 2022, **159**, 433–441.

19 J. R. Howell, M. P. Mengüç, K. Daun, *et al.*, *Thermal radiation heat transfer[M]*, CRC press, 2020.

20 N. Omar, R. Zulkifli and R. Hassan, Development of a virtual laboratory for radiation heat transfer, *Eur. J. Sci. Res.*, 2009, **32**(4), 562–571.

21 R. P. Caren, Thermal radiation between closely spaced metal surfaces at low temperature due to traveling and quasi-stationary components of the radiation field, *Int. J. Heat Mass Transfer*, 1974, **17**(7), 755–765.

22 D. Ouyang, J. Weng, M. Chen, *et al.*, A comparative study on safety and electrochemical characteristics of cylindrical lithium-ion cells with various formats, *Process Saf. Environ. Prot.*, 2022, **161**, 126–135.